**Supporting Information**

# Exploring the Nitric Oxide Dioxygenation (NOD) Reactions of Manganese-peroxo Complexes

Sandip Das[†,‖] Akshaya Keerthi C S[†,‖] Kulbir[†,‖] Shivangi Singh[†], Soumik Roy[†], Raman Singh,[†§] Somnath Ghosh,*[†] Pankaj Kumar*[†]

[†]Department of Chemistry, Indian Institute of Science Education and Research (IISER) Tirupati 517507, India

[§] Division of Chemistry & Toxicology, WTL – Clean & Renewable Energy Pvt. Ltd. New Delhi, India

[‖]equally contributed authors

* To whom correspondence should be addressed.

E-mail: pankaj@iisertirupati.ac.in

## Table of Contents

**Experimental Section**

## Experimental Section

**Materials.** All reagents and solvents obtained from commercial sources (Sigma Aldrich Chemical Co. and Tokyo Chemical Industry) were of the best available purity and were used without further purification unless otherwise indicated. Solvents were dried according to reported literature and distilled under an inert atmosphere before use.[S1] The ligands 3PYENMe and N3PY and complexes **1** and **2** were synthesized using already reported procedures.[S2 & S3]

**Instrumentation.** UV-vis spectra were recorded on an Agilent Cary 8454 diode array spectrometer equipped with a thermostat cell holder (UNISOKU Scientific Instruments) designed for low-temperature experiments. FT-IR spectra in solid form were recorded on the Bruker-Alpha Eco-ATR FTIR spectrometer using the standard KBr disk method. $^{1}$H-NMR spectra were measured with a Bruker model Ascend 400 FT-NMR spectrometer. Electrospray ionization mass spectra (ESI-MS) were recorded on an Agilent Mass Spectrometer (6200 series TOF/6500 series Q-TOF B.08.00) by infusing samples directly into the source using a manual method. The spray voltage was set at 4.2 kV, and the capillary temperature was at 80 °C. Single-crystal XRD data were collected at 100 K on a Bruker X-ray diffractometer (Photon III-Duo) using monochromated MoKα (lambda = 0.7107 Å) radiation.

**Reactivity Studies.** All UV-Vis spectral measurements were performed using a quartz cuvette in $CH_3CN$ at – 40 ℃ to 25 ℃. We performed the reactions under the Ar atmosphere wherever required. All kinetic reactions were run at least three times, and the data reported here are the average outcome for these reactions.

**Labelling ($^{14}$N & $^{15}$N) experiments using FT-IR spectroscopy.** We have recorded the FT-IR spectra of the reaction mixtures in their solid state as KBr pellets to follow the N-atom in the NOD reactions. These reactions were executed under an Ar atmosphere. 20 mM solutions

of **1** and **2** were prepared in $CH_3CN$ in two different vials under an Ar atmosphere at - 40 ℃. Then, they reacted with NO at - 40 ℃. After reaction completion, the samples were dried under a vacuum and washed with $Et_2O$. The FT-IR spectrum of the reaction mixture of **1** with NO showed a characteristic peak at 1385 $cm^{-1}$ for the $Mn^{II}$-nitrato complex (**3**). While the FT-IR spectrum of the reaction mixture of **2** with NO showed a distinct peak at 1384 $cm^{-1}$, which corresponds to the $Mn^{II}$-nitrato complex (**4**). Both these peaks shifted to 1352 $cm^{-1}$ when the reaction mixtures of **1** + $^{15}NO$ and **2** + $^{15}NO$ were analyzed. The change in the IR stretching frequency ($\Delta$ ~ 35 $cm^{-1}$ and ~ 34 $cm^{-1}$) confirmed that an increase in the reduced mass of N-atom (from $^{14}N$ to $^{15}N$) is responsible for decreasing the IR stretching frequency of the $NO_3^-$ functional group.

**$^{15}$N Labelling experiments using ESI-MS spectrometry.** Furthermore, to establish the source of N-atom in the above NOD reactions, we performed the $^{15}N$-labeling experiments and followed them with ESI-MS measurements. For the above experiments, two cuvettes (1 mM, 4 mL) were equipped with $CH_3CN$ solutions of **1** and **2** with an airtight rubber septum under an at – 40 °C Ar atmosphere. These solutions were both reacted with $^{15}NO$ in two separate experiments, and the reactions were monitored by UV-Vis spectroscopy. After the completion of the reactions, the ESI-MS spectra of all reaction mixtures were recorded. The ESI-MS spectrum of the reaction mixture obtained in the reaction of **1** + $^{15}NO$ showed a prominent peak at *m/z* 465.13, whose mass value and isotopic distribution pattern correspond to $[(3PYENMe)Mn^{II}(^{15}NO_3^-)]^+$ (calcd *m/z* 465.13). Whereas the reaction of **2** + $^{15}NO$ showed a prominent peak at *m/z* 445.17, whose mass value and isotopic distribution pattern correspond to $[(N3PY)Mn^{II}(^{15}NO_3^-)]^+$ (calcd *m/z* 445.17). These reactions clearly indicate that N moiety in **3** and **4** are derived from NO moiety in NOD reactivity of **1** and **2** complexes, respectively.

**Magnetic moment calculation and determination of the spin state of Mn-center in complexes 3 & 4**: Evans' method of $^{1}$H-NMR was performed to determine the number of unpaired electrons (spin-state) for Mn-center in complexes **3** & **4** at room temperature[S4-S6]. WILMAD® coaxial insert (with a sealed capillary) tube containing the only $CD_3CN$ solvent (with 1.0 % TMS) was inserted into two different regular NMR tubes containing the complex **3** (4.0 mM in $CD_3CN$, with 0.1 % TMS), and **4** (4.0 mM in $CD_3CN$, with 0.1 % TMS) (Sample was prepared at - 40 °C. and recorded immediately). We have calculated the chemical shift value of the TMS / solvent peak in the presence of complex **3** and **4** concerning that of the TMS / solvent peak in the inner NMR tube. The magnetic moment was calculated using the given equation.

| **3** | **4** |
|---|---|
| $\mu_{eff} = 0.0618(\Delta\nu T / 2fM)^{1/2}$ | $\mu_{eff} = 0.0618(\Delta\nu T / 2fM)1/2$ |
| $\mu_{eff} = 0.0618 * (112 * 298/2 * 400 * 0.004)^{1/2}$ | $\mu_{eff} = 0.0618 * (96 * 298 / 2 * 400 * 0.004)$ |
| $\mu_{eff} = 6.31$ BM | $\mu_{eff} = 5.84$ BM |

Where f = oscillator frequency (MHz) of the superconducting spectrometer, T = absolute temperature, M = molar concentration of the complex, and ν = difference in frequency (Hz) between the two TMS signals. The calculated magnetic moment of complexes **3** and **4** were determined to be 6.31 BM and 5.84 BM, respectively, suggesting the presence of five unpaired electrons in both **3** and **4**.

**Nitrate estimation by modified Griess reagent:** Complexes **1** and **2** were reacted with NO under the Ar atmosphere at – 40 °C in two separate experiments by above demonstrated process. The color of the solution was changed from deep blue to off-white. After completing

both reactions, the reaction mixtures were warmed to room temperature and dried on the rotary evaporator. We added water (5.0 mL) to the dried products, and then a solution of 10 equivaent $Na_2S$ was added, and the reaction mixture was kept for 30 minutes. Manganese precipitates as MnS and is separated by filtration. The organic component of the reaction mixture was separated from the aqueous layer using $CH_2Cl_2$. We diluted the aqueous layer up to 10 mL. To prepare the sample for quantification of $NO_3^-$, 25 μL of this solution was added to a sample vial containing 1.0 mL of freshly prepared modified Griess reagent and then diluted to 2.5 mL by adding $H_2O$. The modified Griess reagent was prepared by mixing sulphanilic acid (0.2 %), naphthylethylenediamine dihydrochloride (0.01%), and $VCl_3$ (0.8 % in 1M HCl) in an aqueous solution. We did not observe any color change immediately, but after keeping the sample overnight, the color changed to violet pink. We have compared the UV-vis spectra of this solution with a calibration plot prepared by employing authentic $NaNO_3$ solutions (SI, Figure S6). The yield of $NO_3^-$ determined by using the modified Griess reagent in the reaction of **1** and **2** with NO was found to be 85 ± 2 % and 90 ± 3 %, respectively.

To obtain the calibration curve, the stock solutions of $NaNO_3$ in various concentrations (0, 0.20, 0.40, 0.60, 0.80, 1.00, 1.20, 1.40, 1.60, 1.80, 2.00 mM) were prepared, and 25 μL of each stock solution was added to a sample vial containing 1.0 mL of fresh prepared modified Griess reagent and then diluted to 2.5 mL by adding $H_2O$. We recorded UV-vis spectra for each standard solution, and a calibration plot was prepared with varying concentrations of $NO_3^-$ (0, 2.0, 4.0, 6.0, 8.0, 10, 12, 14, 16, 18, 20 μM) and the corresponding $\lambda_{max}$ at 550 nm (SI, Figure S6).

**Single-Crystal XRD Studies:** Single-crystal XRD data were collected at 100 K on a Bruker X-ray diffractometer (Photon III-Duo) using monochromated MoKα (lambda =

0.7107 Å) radiation. The collected frames were integrated, scaled, merged, and absorption correction was performed using the program package APEX4 (Bruker 2022) to determine the unit cell. The structure was solved with SHELXS and refined against F2 by weighted full-matrix least squares using SHELXL.[S7] All non-hydrogen atoms were refined with anisotropic displacement parameters. Hydrogen atoms attached to carbon were placed at calculated positions and refined using a riding model. Detailed crystallographic data and structural refinement parameters are summarized in Table T1 – T2. CCDC- 2218826 and 2218827 contain supplementary crystallographic data for this paper. These data can be obtained free of charge from The Cambridge Crystallographic Data Centre.

**References**


S1. W. L. F Armarego, C. L. L Chai, *Purification of Laboratory Chemicals*, 6th ed.; Pergamon Press: Oxford, **2009**.
S2. R. A. Geiger, D. F. Leto, S. Chattopadhyay, P. Dorlet, E. Anxolabéhère-Mallart and T. A. Jackson, *Inorg. Chem.,* **2011**, 50, 10190-10203.
S3. D. D. Narulkar, A. Ansari, A. K. Vardhaman, S. S. Harmalkar, G. Lingamallu, V. M. Dhavale, M. Sankaralingam, S. Das, P. Kumar and S. N. Dhuri, *Dalton Trans.*, 2021, **50**, 2824-2831
S4. D. F. Evans, *J. Chem. Soc*., 2003-2005 (**1959**).
S5. J. Lölinger, & R. Scheffold, Paramagnetic moment measurements by nmr. A microtechnique. *J. Chem. Edu*., 646-647 (**1972**).
S6. D. F. Evans, & D. A. Jakubovic, *J. Chem. Soc. Dalton Trans*. 2927-2933 (**1988**)
S7. G. M. Sheldrick. Crystal Structure Refinement with SHELXL. *Acta Cryst.* **2015**, C71, 3–8.

**Table T1** Crystallographic data for **3** and **4**.

| | **3** | **4** |
|---|---|---|
| Chemical formula | $C_{45}H_{45}BMnN_6O_3$ | $C_{43}H_{49}BMnN_6O_3$ |
| Formula weight | 783.642 | 762.51 |
| Wavelength /Å | 0.71073 | 0.71073 |
| Crystal system | triclinic | monoclinic |
| Space group | P-1 | $P2_{1/c}$ |
| *T*, K | 100.0 | 100.0 |
| *a*, Å | 11.2760(12) | 16.5034(10) |
| *b*, Å | 14.8557(15) | 11.0969(7) |
| *c*, Å | 25.600(3) | 22.2792(13) |
| α, ° | 89.775(4) | 90 |
| β, ° | 84.127(4) | 106.045(2) |
| γ, ° | 67.815(4) | 90 |
| V/ $Å^3$ | 3947.2(7) | 3921.2(4) |
| Z | 42 | 4 |
| Calculated density, $g/cm^3$ | 1.319 | 1.292 |
| Abs. Coeff. $/mm^{-1}$ | 0.384 | 0.384 |
| Reflections collected | 13956 | 131461 |
| Unique reflections | 13956 | 9714 |
| Refinement method | Least-squares on $F^2$ | Least-squares on $F^2$ |
| Data/restraints/parameters | 13956/0/1012 | 9714/104/527 |
| Goodness-of-fit on $F^2$ | 1.105 | 1.031 |
| Final *R* indices [$I > 2\sigma(I)$] | R1 = 0.0732<br>wR2 = 0.2022 | R1 = 0.0377<br>wR2 = 0.0966 |
| *R* indices (all data) | R1 = 0.0807<br>wR2 = 0.2062 | R1 = 0.0411<br>wR2 = 0.0997 |

**Table T2** Selected bond lengths (Å) and bond angles (°) for **3** and **4**.

| **3** | | **4** | |
|---|---|---|---|
| Mn1 N1 | 2.296(4) | Mn1 O1 | 2.211 (13) |
| Mn1 N2 | 2.337(5) | Mn1 O1A | 2.192 (15) |
| Mn1 N3 | 2.284(5) | Mn1 N1 | 2.2308 (13) |
| Mn1 N4 | 2.323(4) | Mn1 N2 | 2.3531(12) |
| Mn1 N5 | 2.295(4) | Mn1 N3 | 2.3015 (13) |
| Mn1 O1 | 2.222(4) | Mn1 N4 | 2.3105 (13) |
| Mn1 O2 | 2.453(4) | Mn1 N5 | 2.2252 (14) |
| O1 N6 | 1.266 (6) | O2 N6 | 1.152 (2) |
| O2 N6 | 1.260 (6) | O3 N6 | 1.189 (2) |
| O3 N6 | 1.240 (6) | O1 N6 | 1.423 (3) |
| N1 Mn1 N2 | 72.33 (15) | O1 Mn1 N1 | 89.38 (8) |
| N3 Mn1 N1 | 104.03 (16) | O1 Mn1 N2 | 152.23 (8) |
| N4 Mn1 N1 | 137.82 (16) | O1 Mn1 N3 | 85.83(7) |
| N5 Mn1 N1 | 88.24 (15) | O1 Mn1 N4 | 93.46 (8) |
| N2 Mn1 O2 | 148.60 (14) | O1 Mn1 N5 | 117.60 (8) |
| N2 Mn1 N3 | 73.87 (16) | N1 Mn1 N2 | 74.14 (4) |
| N2 Mn1 N5 | 105.04 (15) | N1 Mn1 N3 | 106.07 (5) |
| N5 Mn1 N4 | 73.32 (15) | N1 Mn1 N4 | 174.11 (5) |
| N6 O2 Mn1 | 88.5 (3) | N3 Mn1 N2 | 77.78 (4) |
| N6 O1 Mn1 | 99.2 (3) | N3 Mn1 N4 | 79.31 (5) |
| O1 Mn1 O2 | 54.73 (13) | N4 Mn1 N2 | 105.14 (5) |
| O1 Mn1 N3 | 92.86 (15) | N5 Mn1 N1 | 99.38 (5) |
| O1 Mn1 N2 | 147.55 (14) | N5 Mn1 N2 | 87.56 (5) |
| O1 Mn1 N4 | 134.97 (15) | N5 Mn1 N3 | 145.61 (5) |
| O1 MN1 N5 | 94.52 (15) | N5 Mn1 N4 | 74.73 (5) |
| O1 Mn1 N1 | 82.86 (14) | N6 O1 Mn1 | 109.96 (15) |

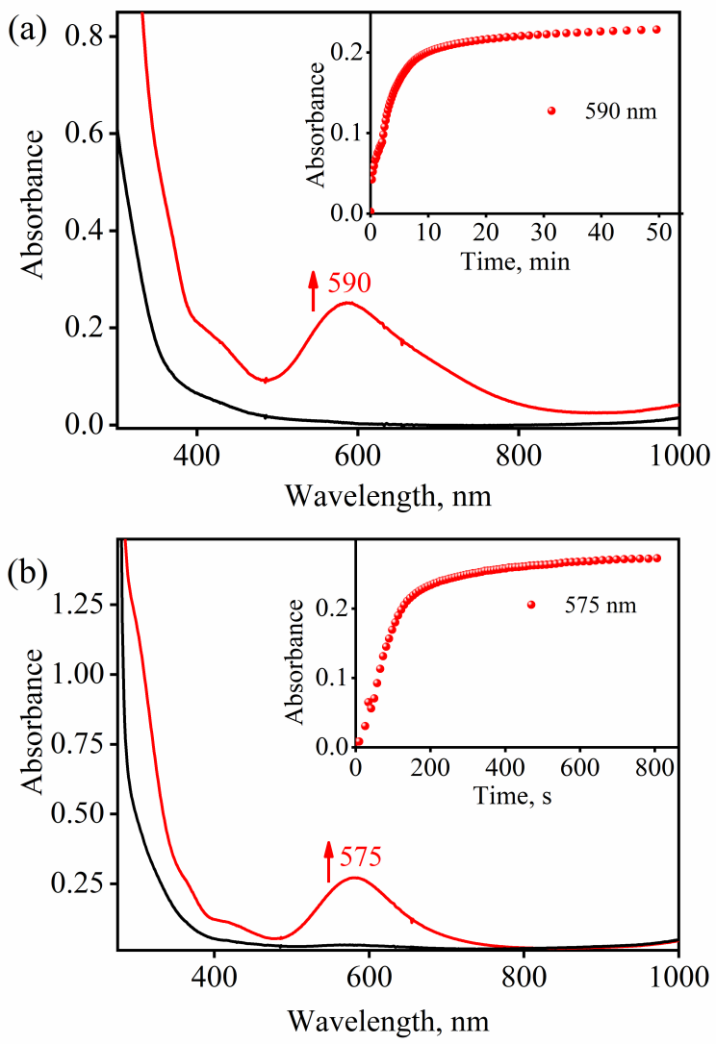


**Figure. S1. (a)** UV-Vis spectral changes of $[(3PYENMe)Mn^{II}]^{2+}$ (2 mM, Black line) upon addition of 1 equiv. $KO_2$ in $CH_3CN$ at - 25 °C, the black line ($[(3PYENMe)Mn^{II}]^{2+}$) changed to a red line (**1**). Inset: The time course of formation of **1** monitored at 590 nm. **(b)** UV-Vis spectral changes of $[(N3PY)Mn^{II}(H_2O)]^{2+}$ (1 mM, Black line) upon addition of 10 equiv. $H_2O_2$ / 5 equiv. $Et_3N$ in $CH_3CN$ at - 25 °C, the black line ($[(N3PY)Mn^{II}(H_2O)]^{2+}$) changed to a red line (**2**). Inset: The time course of formation of **2** monitored at 575 nm.

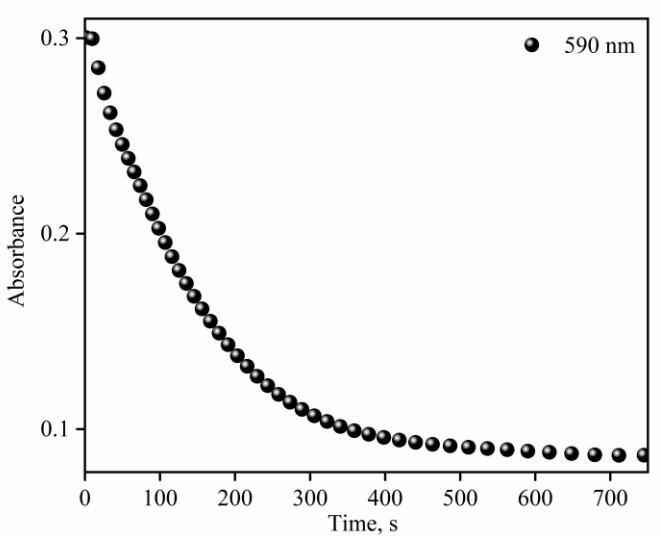


**Figure.S2.** The reaction time course of **1** (2 mM) with NO was monitored at 590 nm at -40 °C in $CH_3CN$ under an Ar atmosphere.

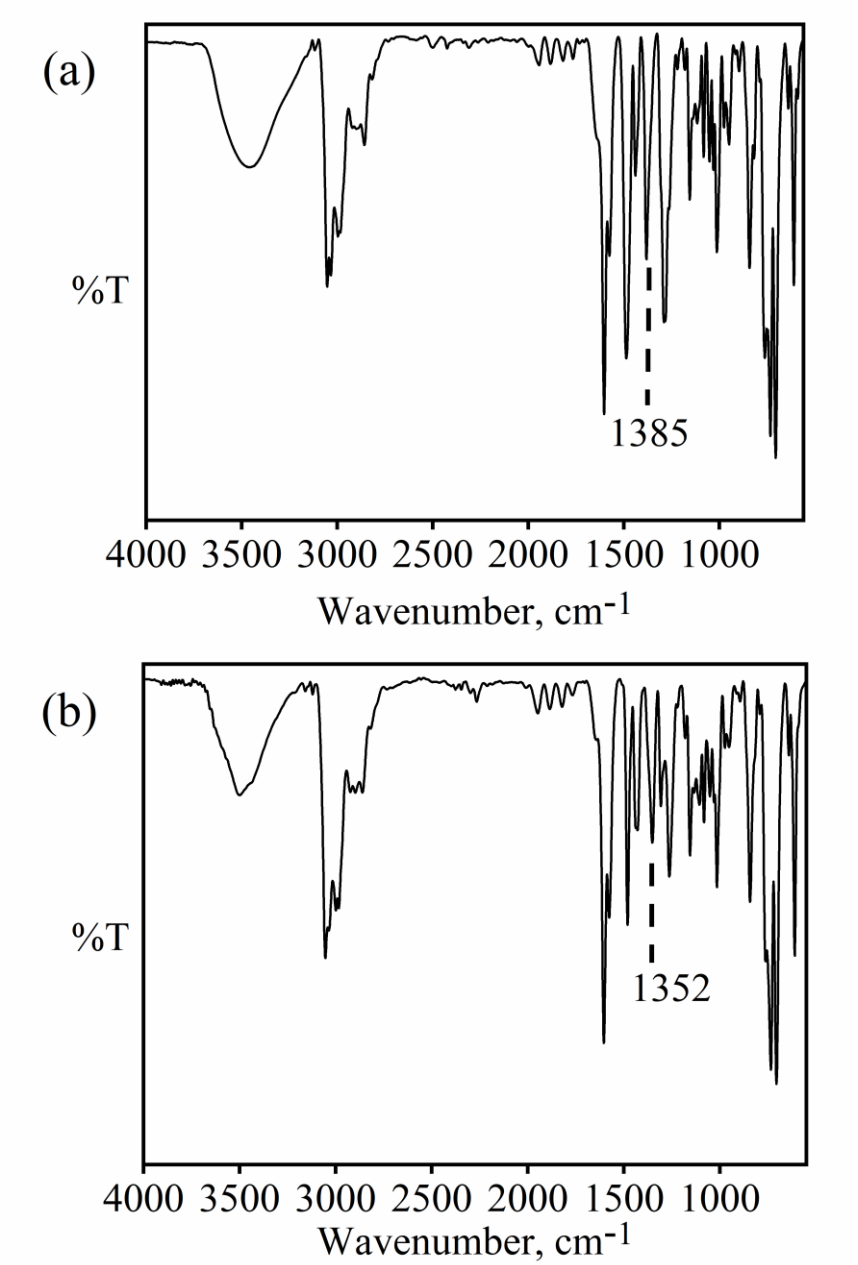


**Figure. S3.** FT-IR spectra of the isolated product obtained from the reaction of (a) **1** + $^{14}$NO (b) **1** + $^{15}$NO were recorded as KBr pellet at 25 °C. The spectra showed the peaks for **3**-$^{14}NO_3^-$ (1385 cm$^{-1}$) and **3**-$^{15}NO_3^-$ (1352 cm$^{-1}$), respectively.

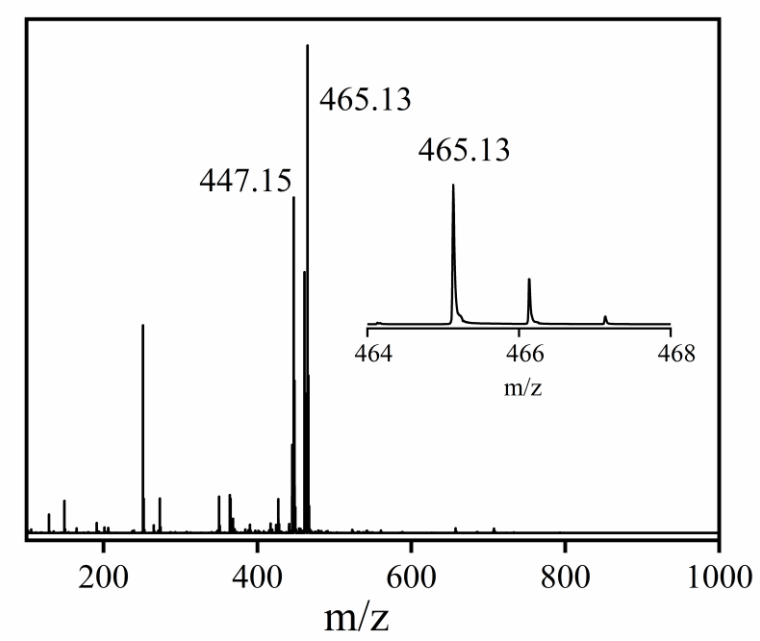


**Figure. S4.** ESI-MS spectrum of complex **3**-$^{15}NO_3^-$ formed in the reaction of **1** with $^{15}NO$ in $CH_3CN$. The peak at *m/z* is assigned to be $[(3PYENMe)Mn(^{15}NO_3^-)]^+$ (calcd: *m/z* 465.13). The inset shows the isotopic distribution pattern of the *m/z* 465.13. The peak at 447.15 is assigned to be $[(3PYENMe)Mn(HCOO^-)]^+$ (calcd: *m/z* 447.15), generated due to the formic acid dilution in the mobile phase.

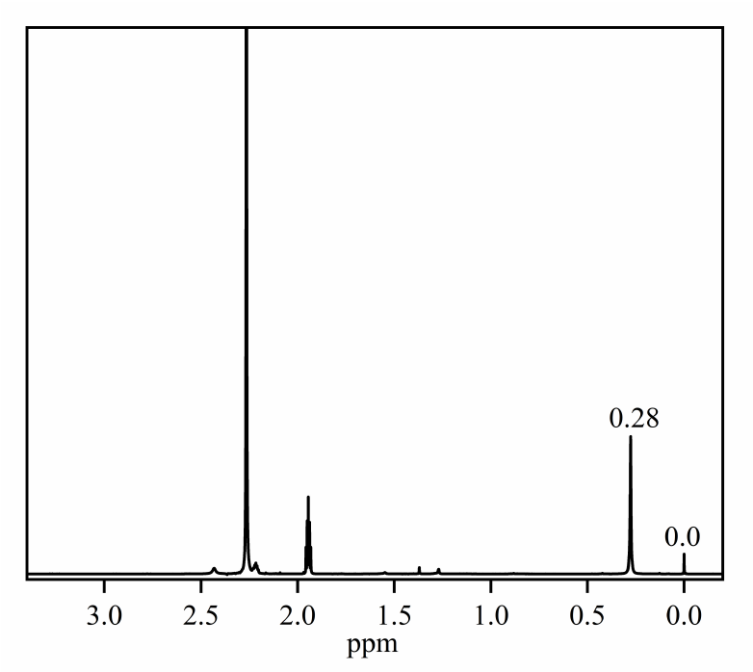


**Figure. S5.** $^{1}$H-NMR (400 MHz) spectra of **3** (4 mM) in $CD_3CN$ (0.1 % TMS), recorded in a coaxial NMR tube, with $CD_3CN$ (1.0 % TMS) inside at 25 °C.

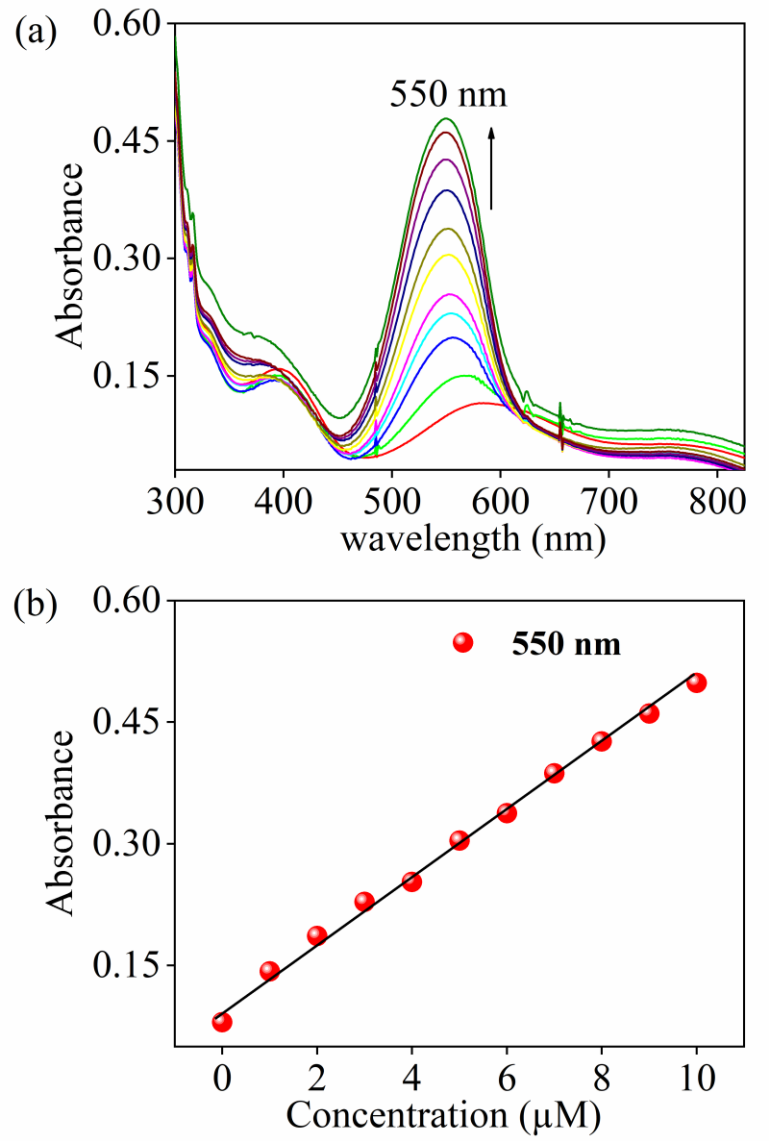


**Figure. S6.** a) UV-vis spectral changes showing the increase in the absorbance at 550 nm (due to the formation of azo dye) upon the addition of $NaNO_3$ solutions in various concentrations (0, 1.0, 2.0, 3.0, 4.0, 5.0, 6.0, 7.0, 8.0, 9.0, 10 μM ) to modified Griess reagent at 25 ˚C. (b) Spectral calibration curve for the peak formation at 550 nm as a function of the concentration of $NaNO_3$ (μM) in increments of 0, 1.0, 2.0, 3.0, 4.0, 5.0, 6.0, 7.0, 8.0, 9.0, 10.

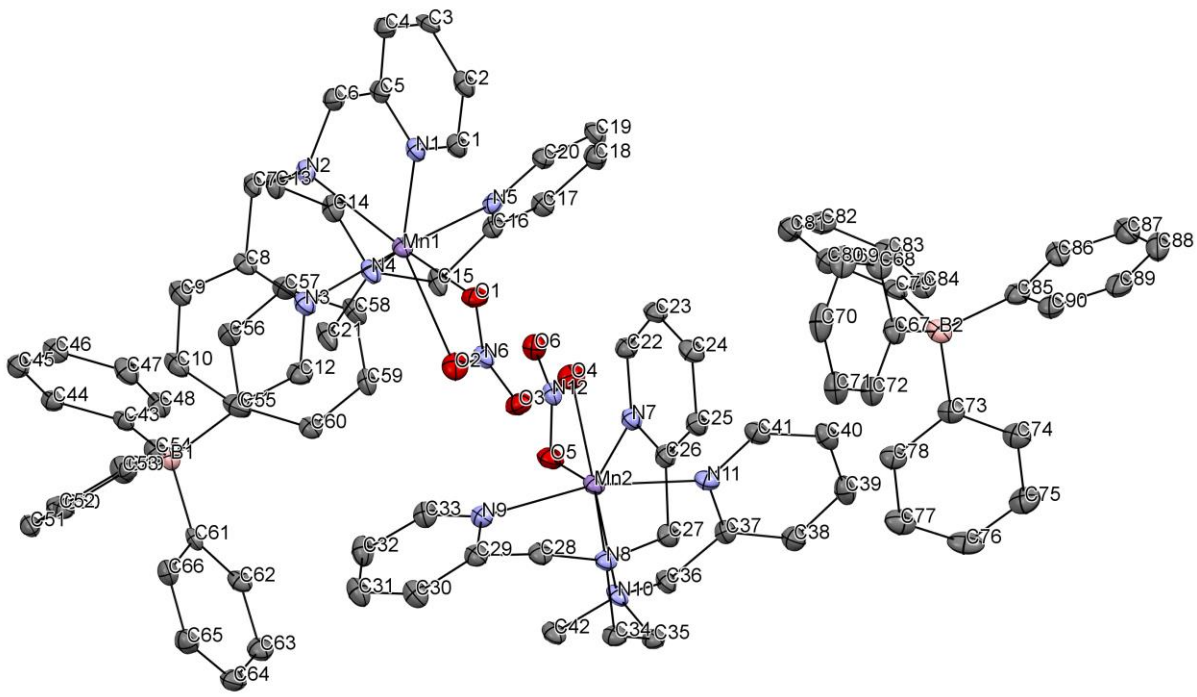


**Figure. S7.** Displacement ellipsoid plot (40 % probability) of **3** at 100 K. H-atoms have been removed for clarity.

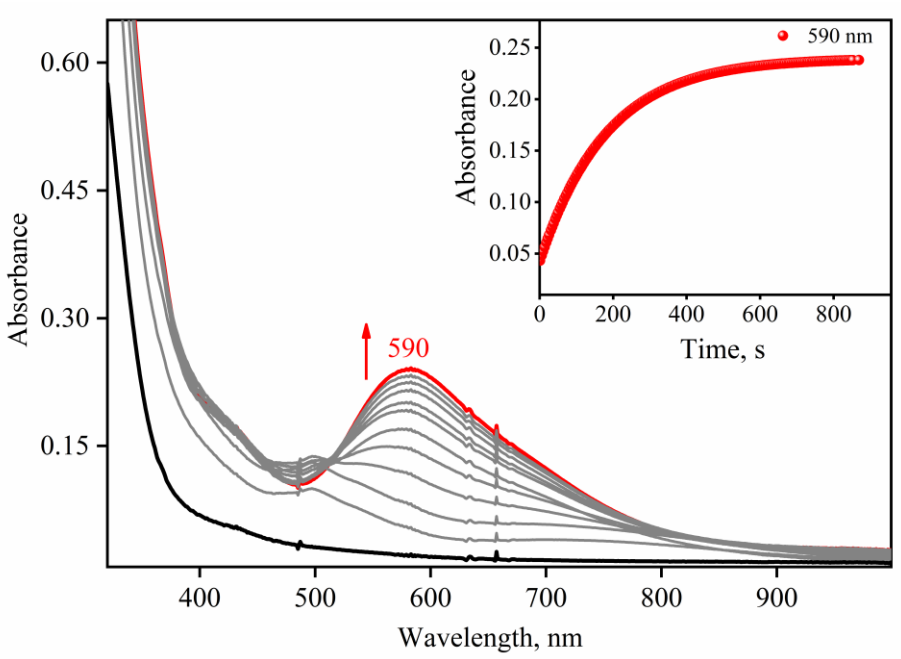


**Figure. S8**: (a) UV-Vis spectral changes of **3** (2 mM, Black line) upon addition of 5 equiv. $H_2O_2$ / 3 equiv. $Et_3N$ in $CH_3CN$ at 0 °C, the black line (**3**) changed to a red line (**1**). Inset: The time course of formation of **1** monitored at 590 nm.

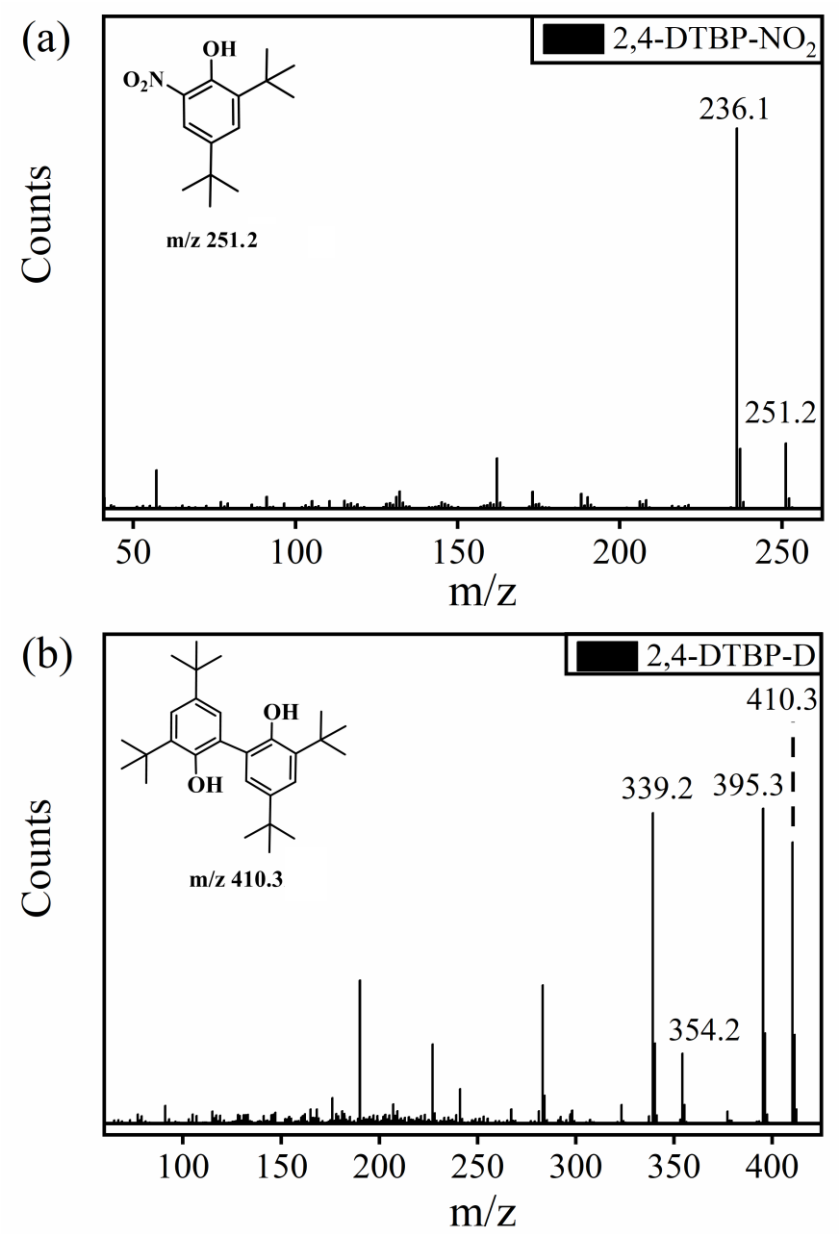


**Figure. S9.** GC-MS characterization of (a) nitro-2,4-DTBP ($NO_2$-2,4-DTBP): The peaks at *m/z* 251.2 and 236.1 are assigned to be nitro-2,4-DTBP and loss of $CH_3$ from nitro-2,4-DTBP. (b) 2,4-DTBP-dimer (2,4-DTBP-D); the peaks at *m/z* 410.3, 395.3, 339.2 and 354.2 are assigned to be 2,4-DTBP-D, loss of $CH_3$, loss of $C_4H_9$ and $C_5H_{11}$ from 2,4-DTBP-D respectively. The peaks were compared with the NIST standard library.

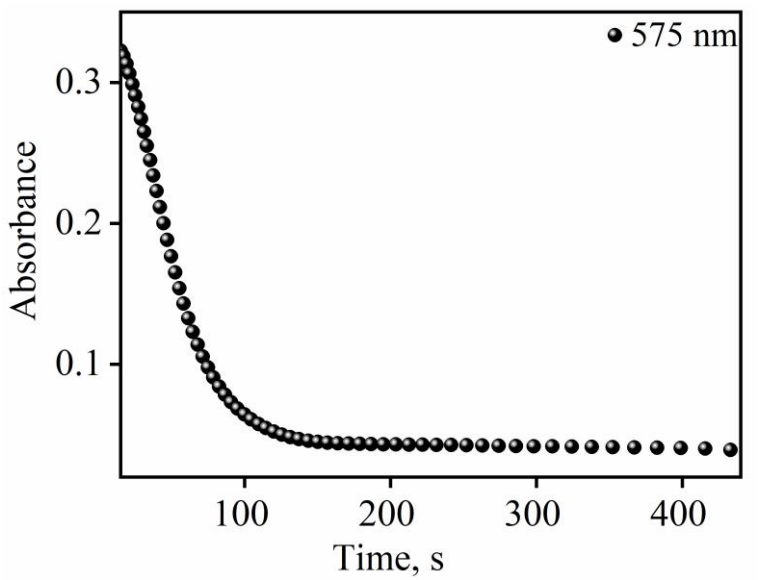


**Figure. S10.** The reaction time course of **2** (1 mM) with NO was monitored at 575 nm at -40°C in $CH_3CN$ under an Ar atmosphere.

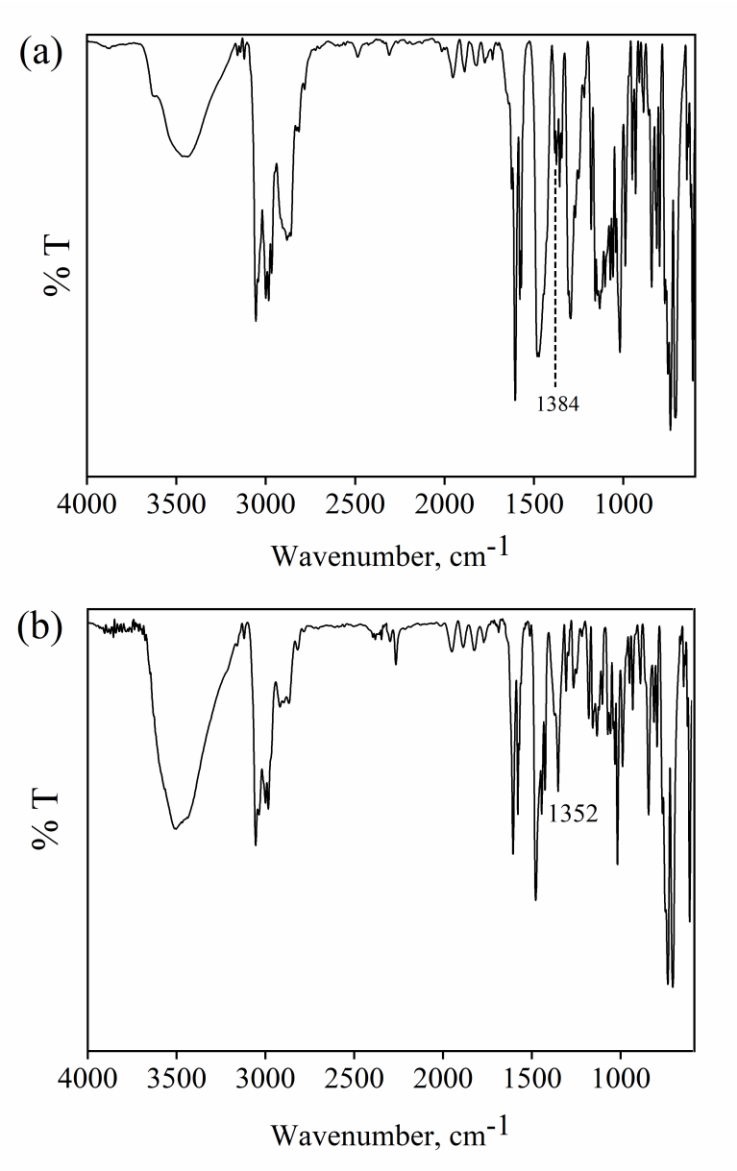


**Figure. S11.** FT-IR spectra of the isolated product obtained from the reaction of (a) **2** + $^{14}NO$ (b) **2** + $^{15}NO$ were recorded as KBr pellet at 298 K. The spectrum showed the peaks for **4**-$^{14}NO_3^-$ (1384 $cm^{-1}$) and **4**-$^{15}NO_3^-$ (1352 $cm^{-1}$), respectively.

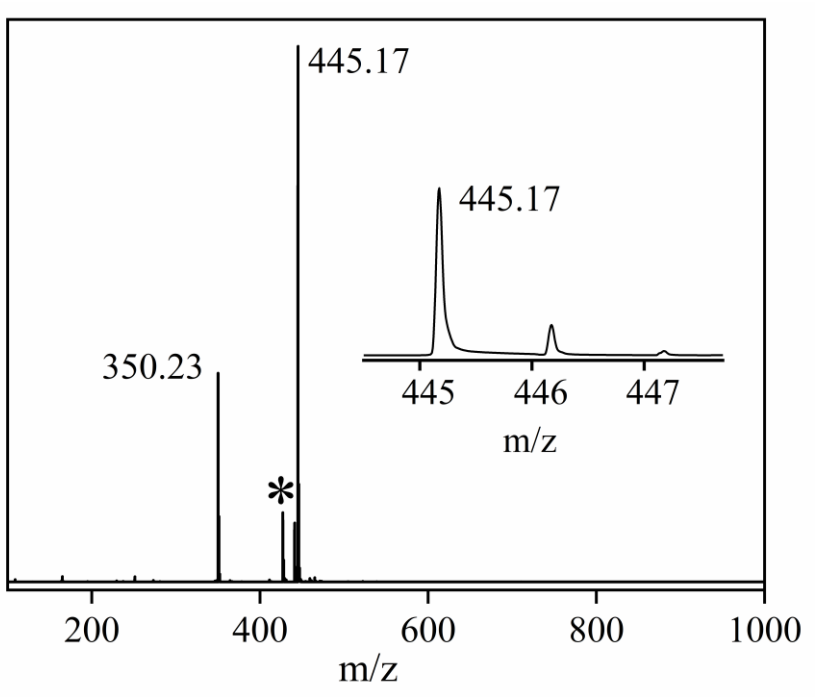


**Figure. S12.** ESI-MS spectrum of complex **4**-$^{15}NO_3^-$ formed in the reaction of **2** with $^{15}NO$ in $CH_3CN$. The peak at *m/z* 445.17 is assigned to be $[(N3PY)Mn^{II}(^{15}NO_3^-)]^+$ (calcd: *m/z* 445.17). The inset shows the isotopic distribution pattern of the *m/z* 445.17. The peak at 350.23 is assigned to be $[N3PY(Na)]^+$ (calcd: *m/z* 350.23). The peak marked with an asterisk at 427.18 is assigned to be $[(N3PY)Mn^{II}(HCOO^-)]^+$ (calcd: *m/z* 427.18), generated due to the formic acid dilution in the mobile phase.

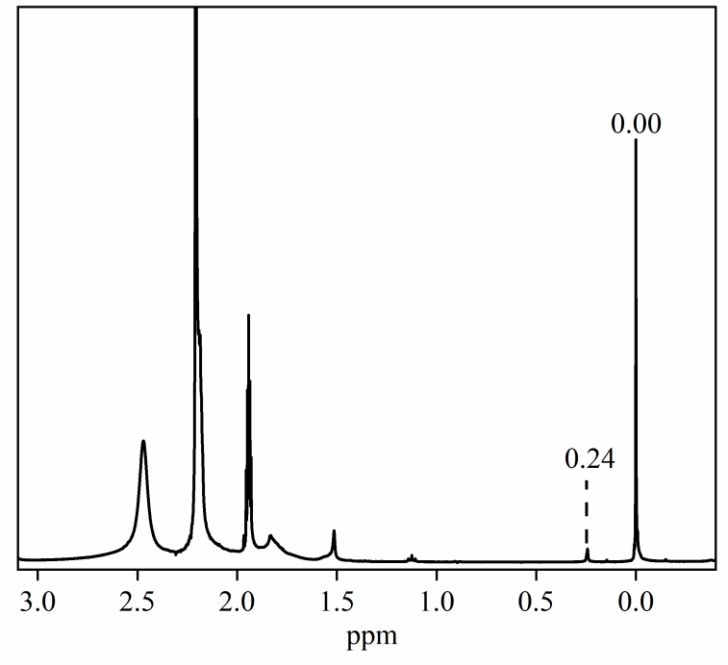


**Figure. S13.** $^{1}$H-NMR (400 MHz) spectrum of **4** (4 mM) in $CD_3CN$ (0.1 % TMS), recorded in a coaxial NMR tube, with $CD_3CN$ (1.0 % TMS) inside at 25 °C.

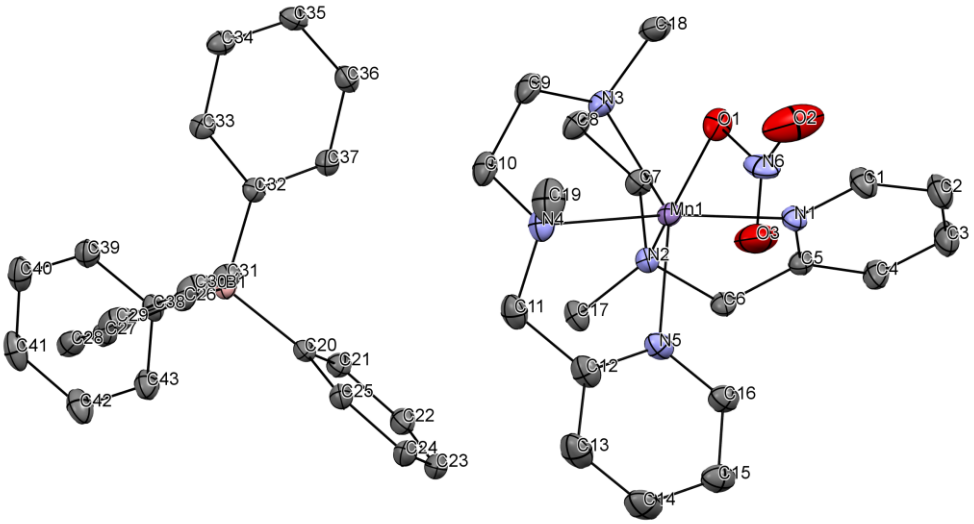


**Figure. S14.** Displacement ellipsoid plot (40 % probability) of **4** at 100 K. disordered N, O-atoms and H-atoms have been removed for clarity.

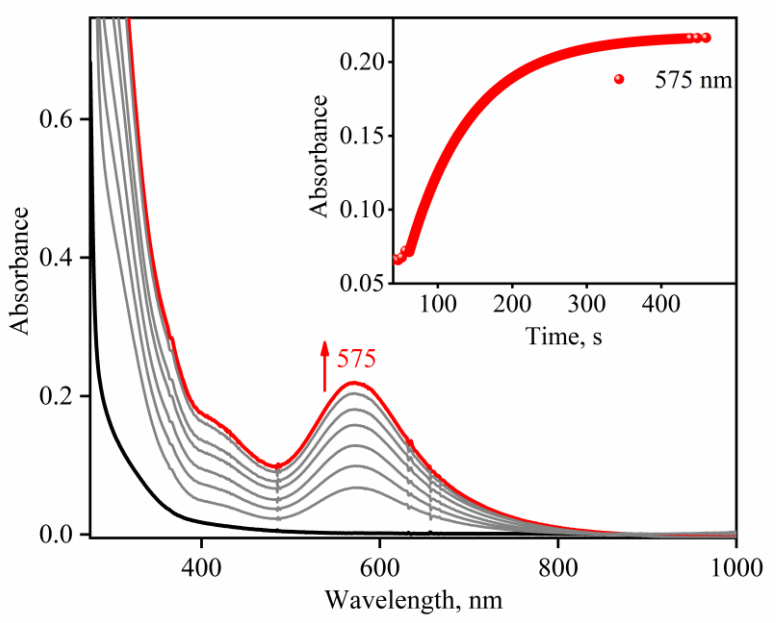


**Figure. S15.** (a) UV-Vis spectral changes of **4** (1 mM, Black line) upon addition of 3 equiv. $H_2O_2$ / 1.5 equiv. $Et_3N$ in $CH_3CN$ at 0 °C, the black line (**4**) changed to the red line (**2**). Inset: The time course of formation of **2** monitored at 575 nm.

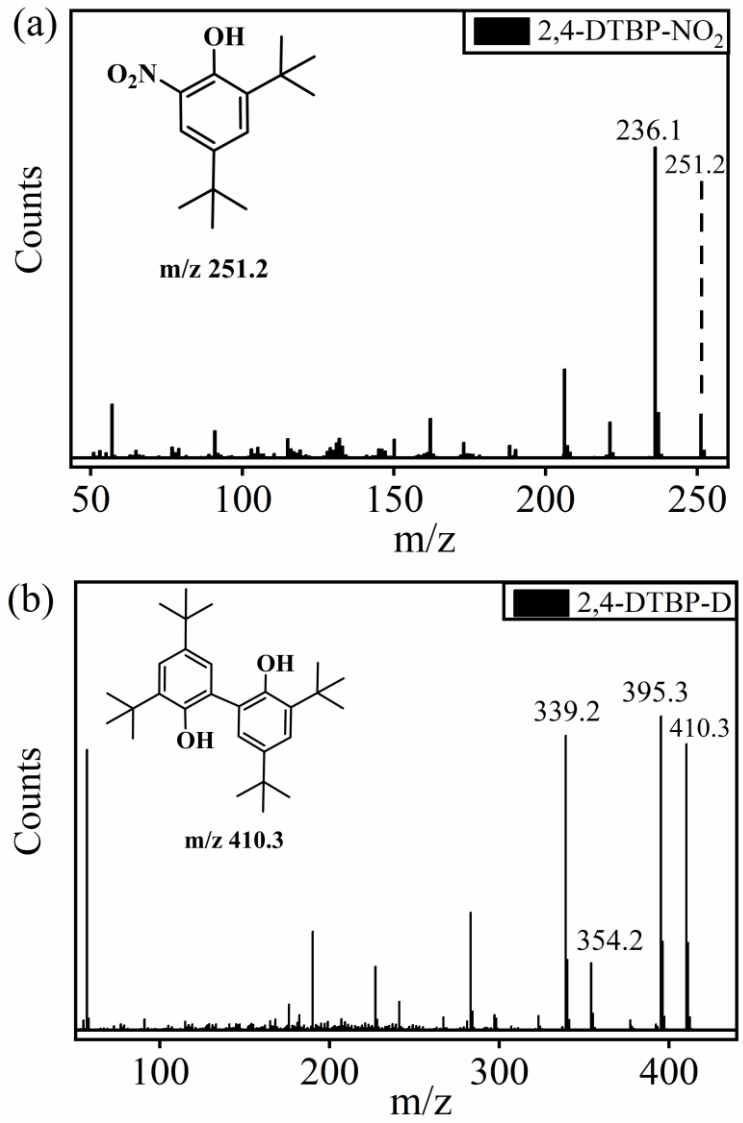


**Figure. S16.** GC-MS characterization of (a) nitro-2,4-DTBP ($NO_2$-2,4-DTBP): The peaks at *m/z* 251.2 and 236.1 are assigned to be nitro-2,4-DTBP and loss of $CH_3$ from nitro-2,4-DTBP. (b) 2,4-DTBP-dimer (2,4-DTBP-D); the peaks at *m/z* 410.3, 395.3, 339.2 and 354.2 are assigned to be 2,4-DTBP-D, loss of $CH_3$, loss of $C_4H_9$ and $C_5H_{11}$ from 2,4-DTBP-D. The peaks were compared with the NIST standard library.

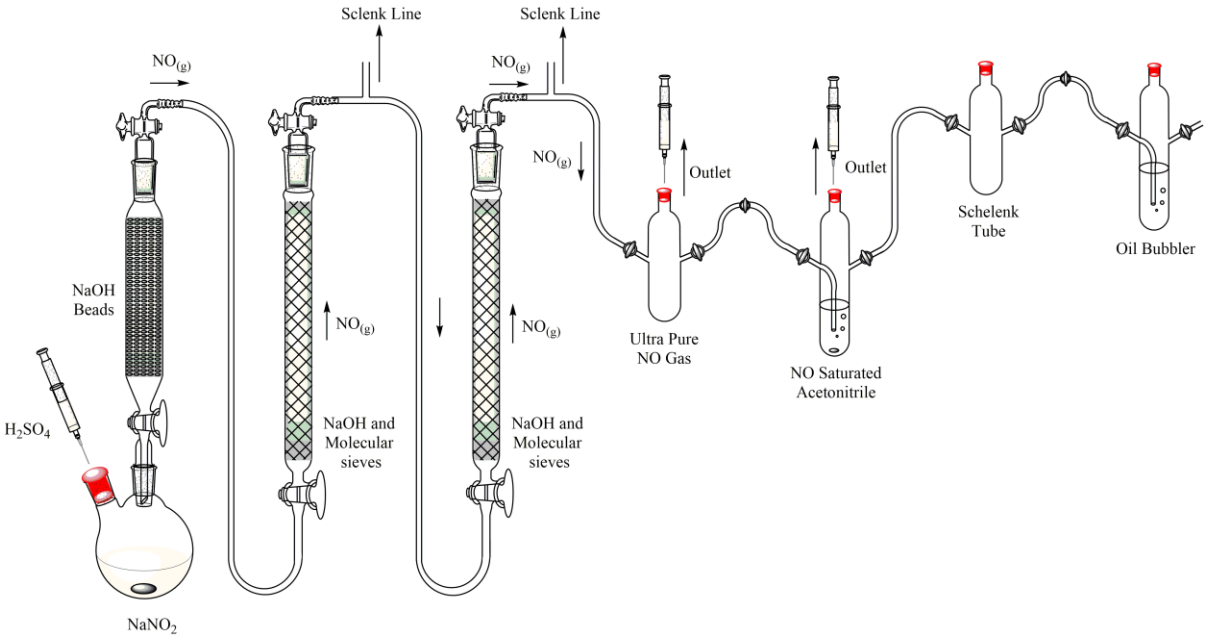


**Figure S17.** Schematic diagram showing the generation and purification setup for NO.